Biomechanics and Modeling in Mechanobiology manuscript No.

Modeling cell proliferation for simulating three-dimensional tissue morphogenesis based on a reversible network reconnection framework

Satoru Okuda · Yasuhiro Inoue · Mototsugu Eiraku · Yoshiki Sasai · Taiji Adachi

Received: 7 September 2012 / Accepted: 14 November 2012 / Published online: 30 November 2012

Abstract Tissue morphogenesis in multicellular organisms is accompanied by proliferative cell behaviors: cell division (increase in cell number after each cell cycle) and cell growth (increase in cell volume during each cell cycle). These proliferative cell behaviors can be regulated by multicellular dynamics to achieve proper tissue sizes and shapes in three-dimensional (3D) space. To analyze multicellular dynamics, a reversible network reconnection (RNR) model has been suggested, in which each cell shape is expressed by a single polyhedron. In this study, to apply the RNR model to simulate tissue morphogenesis involving proliferative cell behaviors, we model cell proliferation based on a RNR model framework. In this model, cell division was expressed by dividing a polyhedron at a planar surface for which cell division behaviors were characterized by three quantities: timing, intracellular position, and normal direction of the dividing plane. In addition, cell growth was expressed by volume growth as a function of individual cell times within their respective cell cycles. Numerical simulations using the proposed model showed that tissues grew during successive cell divisions with several cell cycle times. During these processes, the cell number in tissues increased while maintaining individual cell size and shape. Furthermore, tissue morphology dramatically changed based on different regulations of cell division directions. Thus, the proposed model successfully provided a basis for expressing proliferative cell behaviors during morphogenesis based on a RNR model framework.

Keywords Tissue morphogenesis · Cell proliferation · Cell division · Multicellular dynamics · Three-dimensional vertex model · Reversible network reconnection model · Computational biomechanics · Developmental biomechanics

S. Okuda · Y. Inoue · T. Adachi
Department of Biomechanics, Institute for Frontier Medical Sciences, Kyoto University
53 Kawahara-cho, Shogoin, Sakyo-ku, Kyoto 606-8507, Japan
E-mail: adachi@frontier.kyoto-u.ac.jp

Y. Inoue
E-mail: inoue@frontier.kyoto-u.ac.jp

M. Eiraku
Four-Dimensional Tissue Analysis Unit, Center for Developmental Biology, RIKEN, Kobe, Japan

Y. Sasai
Organogenesis and Neurogenesis Group, Center for Developmental Biology, RIKEN, Kobe, Japan

1 Introduction

During tissue morphogenesis in multicellular organisms, tissues grow primarily as a result of successive rounds of cell proliferation. In growing tissues, the cell number increases after each cell division, and the decrease in cell size after cell division is recovered by cell growth. In particular, because the size of each cell is approximately maintained during many developmental processes, the size of whole tissue dramatically increases in three-dimensional (3D) space. Thus, proliferative cell behaviors are fundamental during tissue morphogenesis.

Recent experimental and theoretical studies have suggested how proliferative cell behaviors mechanically affect tissue morphogenesis. For example, the rates of cell divisions can be spatially non-uniform in tissues (Eiraku et al. 2011, 2012), and this spatial non-uniformity can enforce an inhomogeneity in tissue shape. Moreover, asymmetric cell divisions (Lechler and Fuchs 2005) can introduce geometrical differences, such as cell sizes between daughter cells after cell division, which leads

to inhomogeneity in cell configurations. Furthermore, globally aligned directions of cell divisions (Gong and Fraser 2004; Heisenberg et al. 2000; Reddy, et al. 2004) can induce anisotropic tissue extensions. Such directionality of cell divisions has been suggested to be sufficient for tissue morphogenesis of the organs in Drosophila (Baena-López, et al. 2005). These mechanical effects of proliferative cell behaviors can be regulated to achieve proper tissue morphology.

During these processes of tissue morphogenesis that are accompanied by proliferative cell behaviors, multicellular dynamics are commonly observed, such as cell deformation and rearrangement (Davies 2005; Farhadifar et al. 2007; Ingber and Mammoto 2010; Rauzi et al. 2008; Staple et al. 2010; Weliky and Oster 1990; Lecuit and Lenne 2007; Lecuit et al. 2010; Friedlander et al. 1989; Lecuit et al. 2008). These multicellular dynamics are necessary for the formation of complex tissues and organs. To obtain a better understanding of tissue morphogenesis, it is necessary to determine the mechanical effects of proliferative cell behaviors on multicellular dynamics.

3D vertex models have been proposed for analyzing multicellular dynamics (Honda et al. 2004, 2008a,b; Okuda et al. 2012). In a 3D vertex model, each cell shape is represented by a single polyhedron, and a multicellular aggregate is represented by a single network comprising vertices and edges. In addition, cell deformations are expressed by vertex dynamics, and cell rearrangements are expressed by reconnecting local network patterns. A 3D vertex model (Honda et al. 2004) has been successfully used to analyze the polarization of early embryos (Honda et al. 2008a) and convergent extensions of tissues (Honda et al. 2008b). In addition, to apply 3D vertex models to simulate the complex tissue deformations during dynamic morphogenesis, a reversible network reconnection (RNR) model has been proposed (Okuda et al. 2012). In such vertex model frameworks, cell division has been modeled and implemented into two-dimensional vertex models (Honda et al. 1984). It has enabled to analyze mechanical effects of cell proliferation in flat tissues with monolayer structure. Thus, to investigate mechanical effects of cell proliferation in tissues curved in 3D space or tissues with multilayer structure, it is a challenging problem to express cell proliferation in a 3D vertex model framework.

In this study, to analyze the mechanical effects of proliferative cell behaviors, we model cell proliferation based on a RNR model framework. In our proposed model, cell division is expressed by dividing a polyhedron at a planar surface for which cell division behaviors are characterized by three quantities: timing; intracellular position; and normal direction of the dividing plane. These are expressed in terms of how to divide each polyhedron at a single plane. In addition, cell growth is expressed by potential energy that is a function of individual cell times within their respective cell cycles. To establish that proliferative cell behaviors are expressed, the cell number in tissues, cell size, and cell shape were observed. Moreover, the differences in tissue morphology based on different regulations for assigning a cell division direction are discussed. Application areas and future perspectives of our proposed model have also been discussed.

2 Modeling cell proliferation based on a RNR framework

2.1 Dynamics of multicellular aggregates

Tissue is an aggregate consisting of a certain cell number (Fig. 1a). The RNR model (Okuda et al. 2012) expresses a single cell shape by a polyhedron (Figs. 1b and e). The polyhedron includes vertices and edges that are shared by neighboring polyhedrons. These vertices and edges comprise a network that represents the entire shape of the aggregate (Figs. 1a and d). In this network, each vertex is connected to four edges, no more and no less. Also, neighboring polyhedrons are compartmentalized by these polygonal faces.

To express the multicellular dynamics within aggregates, an equation for the motion of the ith vertex is introduced by

$$\eta \frac{d\boldsymbol{r}_i}{dt} = -\frac{\partial U}{\partial \boldsymbol{r}_i}. \tag{1}$$

The left hand side of Eq. (1) indicates a frictional force exerted on the ith vertex, where η is a friction coefficient and $\boldsymbol{r}_i$ is the position vector of the ith vertex. The right hand side of Eq. (1) indicates a conservative force acting on the ith vertex, where U is potential energy that represents a cell's potential energy. In addition, cell rearrangements within an aggregate are expressed by reconnecting local network patterns (Okuda et al. 2012).

2.2 Proliferative cell behaviors

Proliferative cell behaviors are characterized by cell division and growth (Figs. 1b and c). In particular, cell division behaviors are characterized by three quantities: timing, intracellular position, and normal direction of the dividing plane. Based on a RNR model framework, these proliferative cell behaviors should be expressed from two perspectives: topological and physical. From the topological perspective, because a single

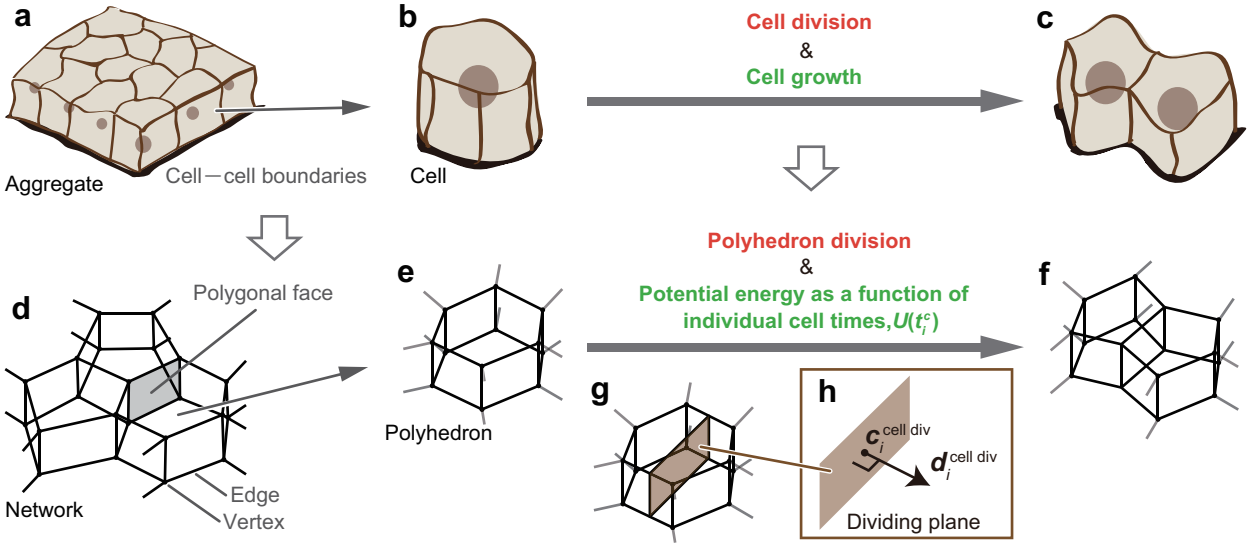

Fig. 1 Modeling cell proliferation based on a RNR framework. **a** Cell aggregate in which cells are tightly packed and adhere at cell–cell boundaries. **b** Single cell embedded within an aggregate. **c** Two deforming daughter cells accompanied by cell growth throughout the cell cycle. **d** Network representing an aggregate in a RNR model framework. The network comprises vertices and edges (solid lines). Cells are compartmentalized by polygonal faces (gray area) that represent cell–cell boundaries. **e** Single polyhedron representing a single cell. **f** Two polyhedrons. Cell growth (increase in cell volume during the cell cycle) is expressed by potential energy that is a function of individual cell times within their respective cell cycles, $U(t_i^c)$. **g** Two polyhedrons representing two daughter cells shortly after a single mother cell has divided. Cell division (increase in cell number after a cell cycle) is represented by dividing a polyhedron at a dividing plane where a new polygonal face is introduced (brown area). **h** Dividing plane. The dividing plane of the ith cell is normal to the direction of the vector $\boldsymbol{d}_i^{\text{cell div}}$ and passes through the position of the vector $\boldsymbol{c}_i^{\text{cell div}}$.

cell is represented by a single polyhedron based on the RNR model framework, a polyhedron is divided into two polyhedrons. From the physical perspective, cell growth can be expressed by a potential energy function. Thus, we have provided separate topological and physical models of cell division.

First, for topological modeling of the cell division process, each polyhedron is divided at a single plane, hereafter called dividing plane (Fig. 1g), and a new polygonal face is introduced on the dividing plane inside the polyhedron. The dividing plane is defined as passing through a position vector, $\boldsymbol{c}_i^{\text{cell div}}$, and is normal to a direction vector, $\boldsymbol{d}_i^{\text{cell div}}$ (Fig. 1h). Here, the position vector $\boldsymbol{c}_i^{\text{cell div}}$ is defined as being inside of the ith cell volume and the direction vector $\boldsymbol{d}_i^{\text{cell div}}$ is defined as a unit vector normal to the dividing plane.

Under procedure for dividing a polyhedron, the dividing plane intersects the polyhedron at several edges (Fig. 1g). These edges are sequentially linked as a ring-like strand on the plane, and compose a single polygon, which is defined as a new polygonal face. This polygonal face separates the polyhedron into two polyhedrons, which are defined as daughter cells.

Next, for physical modeling of cell growth, cell time t_i^c is defined as the time counted since the ith cell was generated by a cell division. Defining $\{t_i^c\} = \{t_0^c, t_1^c, t_2^c, \cdots, t_i^c, \cdots, t_n^c\}$, the potential energy $U(\{t_i^c\})$ was introduced as a function of cell times $\{t_i^c\}$ within the particular cell cycle. In addition, to express the timing of cell division, cell division time is introduced, $\tau_i^{\text{cell div}}$. Constant $\tau_i^{\text{cell div}}$ is defined as the time of the ith cell division that is counted since the ith cell was generated.

Using t_i^c and $\tau_i^{\text{cell div}}$, potential energy, U, is expressed by

$$U(\{t_i^c\}) = U^{\text{cell}} + U^{\text{cell–cell}} + U^{\text{cell–ext}}, \tag{2}$$

$$U^{\text{cell}}(\{t_i^c\}) = \sum_j^{\text{cell}} u_j^{\text{cell}}\left(\boldsymbol{r}_k, t_j^c\right)\delta_j^*, \tag{3}$$

$$U^{\text{cell–cell}}(\{t_i^c\}) = \sum_j^{\text{cell}}\sum_k^{\text{cell}} u_{jk}^{\text{cell–cell}}\left(\boldsymbol{r}_l, t_j^c, t_k^c\right)\delta_j^*\delta_k^*, \tag{4}$$

$$U^{\text{cell–ext}}(\{t_i^c\}) = \sum_j^{\text{cell}} u_j^{\text{cell–ext}}\left(\boldsymbol{r}_k, t_j^c\right)\delta_j^*, \tag{5}$$

where $\delta_j^* = \delta_{\lfloor t_j^c/\tau_j^{\text{cell div}}\rfloor 0}$. The functions $\delta_{\alpha\beta}$ and $\lfloor\ldots\rfloor$ indicate Kronecker's delta and floor functions, respectively. In Eqs. (3), (4), and (5), $\sum^{\text{cell}}$ indicates summations for all cells. Potential energy u_j^{cell} represents some energy of the jth cell, such as volume elasticity, surface elasticity, apical constriction, and other effects of intracellular structures and activities. The potential

energy $u_{jk}^{\text{cell–cell}}$ indicates some energy between the jth and kth cells, such as cell-cell adhesions at intercellular junctions. The potential energy $u_j^{\text{cell–ext}}$ indicates some energy between the jth cell and extracellular components, such as extracellular matrixes, basement membranes, and solvent liquids. Assuming that a cell's potential energy can be simply expressed by a single-well potential, a cell's potential energy depends on mechanical properties and the reference state of this potential. Hence, cell growth is expressed by time-variations in these mechanical properties and the reference state.

3 Introducing cell behaviors into our proposed model

To demonstrate simulations using our proposed model, the morphodynamics of growing tissues are simulated. For these simulations, cell division behaviors and the potential energies of proliferating cells are simply expressed as follows.

3.1 Cell division behaviors

In our proposed model, cell division behaviors are determined by regulations that provide $\tau_i^{\text{cell div}}$, $\boldsymbol{c}_i^{\text{cell div}}$, and $\boldsymbol{d}_i^{\text{cell div}}$.

3.1.1 Timing of cell division

Timing of cell division, $\tau_i^{\text{cell div}}$, was determined so as to be cell cycle independent of the cell mechanical state. Because cell cycles have some time variations, each cell division time is simply expressed so as to satisfy

$$\left\langle \tau_i^{\text{cell div}} \right\rangle = \tau_{\text{ave}}^{\text{cell cycle}}, \tag{6}$$

$$\left\langle \tau_i^{\text{cell div}} \tau_j^{\text{cell div}} \right\rangle = \left(\tau_{\text{sd}}^{\text{cell cycle}} \right)^2 \delta_{ij}, \tag{7}$$

where $\langle ... \rangle$ indicates the statistical average. The constants $\tau_{\text{ave}}^{\text{cell cycle}}$ and $\tau_{\text{sd}}^{\text{cell cycle}}$ indicate the average and standard deviation of cell division times, respectively. Moreover, to express cell growth, the cell cycle was separated into four states: I, II, III, and IV. The time ratios of states I, II, III, and IV were denoted by ψ^{I}, ψ^{II}, ψ^{III}, and ψ^{IV} (≥ 0, $\psi^{\text{I}} + \psi^{\text{II}} + \psi^{\text{III}} + \psi^{\text{IV}} = 1$), respectively.

3.1.2 Intracellular position of cell division

Assuming symmetric cell divisions, the intracellular position of cell division $\boldsymbol{c}_i^{\text{cell div}}$ (Fig. 1h) was determined to be the dividing plane that passes through the center of inertia of the ith cell: $\boldsymbol{c}_i^{\text{cell div}} = \boldsymbol{g}_i^{\text{c}}$. Here, $\boldsymbol{g}_i^{\text{c}}$ indicates the position vector of the center of inertia of the ith cell, of which definition is given in the previous study (Okuda et al. 2012) (Fig. 2a).

3.1.3 Direction of cell division

Direction of cell division, $\boldsymbol{d}_i^{\text{cell div}}$ (Fig. 1h), depends on cell polarity. For example, epithelial cells have an epithelial polarity and many epithelial tissues tend to maintain their monolayer structures (Davies 2005). Thus, in the simulations, assuming that cells divide normal to a tissue surface and to determine a cell's polarity, reference surfaces in Fig. 2a were defined as a part of the cell surface. If the ith cell includes a reference surface (hereafter called case $\Omega_i^{\text{ref surf}}$), the cell division direction was determined normal to this reference surface. Here the normal direction at the ith cell, $\boldsymbol{d}_i^{\text{ref surf}}$ (Fig. 2b), was defined as follows: $\boldsymbol{d}_i^{\text{ref surf}} = \left(\boldsymbol{r}_i^{\text{ref surf}} - \boldsymbol{g}_i^{\text{c}}\right) / \left|\boldsymbol{r}_i^{\text{ref surf}} - \boldsymbol{g}_i^{\text{c}}\right|$, where vector $\boldsymbol{r}_i^{\text{ref surf}}$ indicates the center point of a reference surface at the ith cell. The center point of a reference surface, $\boldsymbol{r}_i^{\text{ref surf}}$, is determined as the center point of its polygonal face, as described in a previous study (Okuda et al. 2012). In contrast, when the ith cell does not include any reference surface (hereafter called case $\overline{\Omega}_i^{\text{ref surf}}$), $\boldsymbol{d}_i^{\text{ref surf}}$ is not defined. In this case, the ith cell is not regarded to have epithelial polarity.

In addition to epithelial cell polarity, the direction of cell division, $\boldsymbol{d}_i^{\text{cell div}}$, was also determined by chemical and mechanical factors (Gibson et al. 2011; Siller et al. 2006; Poulson and Lechler 2010). As characteristic examples, cell divisions can be adaptively oriented according to individual cell shapes (Gibson et al. 2011). Moreover, these directions can be aligned by globally polarized distributions of intracellular molecules (Siller et al. 2006; Poulson and Lechler 2010). To demonstrate that our proposed model can express the various directionalities of cell division, $\boldsymbol{d}_i^{\text{cell div}}$, is given according to the following two regulations.

Local regulation: The directions of cell divisions are locally determined according to individual cell shapes. As a typical example, it is determined to be directed toward the longest axis of individual cell shapes. Then, vector $\boldsymbol{d}_i^{\text{cell div}}$ is an eigenvector that corresponds to the minimum eigenvalue of an inertia tensor of the ith cell, denoted by $\boldsymbol{T}_i^{\text{ci}}$. To reflect the directionality of cell shapes into cell division directions, tensor $\boldsymbol{T}_i^{\text{ci}}$ is derived for cases $\Omega_i^{\text{ref surf}}$ and $\overline{\Omega}_i^{\text{ref surf}}$. For case $\Omega_i^{\text{ref surf}}$, tensor $\boldsymbol{T}_i^{\text{ci}}$ is directly derived from the ith cell shape. In contrast, for case $\overline{\Omega}_i^{\text{ref surf}}$, tensor $\boldsymbol{T}_i^{\text{ci}}$ is derived from the ith cell shape projected onto a plane normal to $\boldsymbol{d}_i^{\text{ref surf}}$.

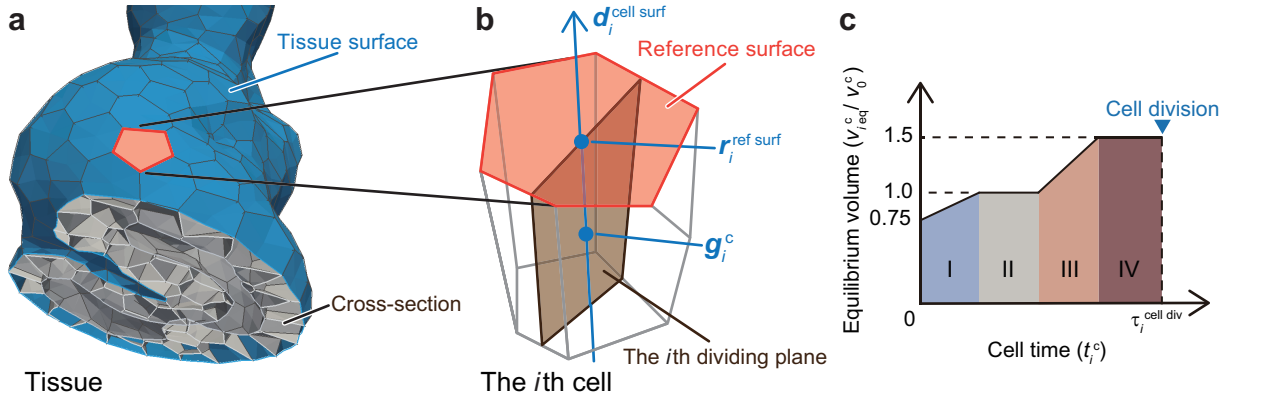

Fig. 2 Proliferative cell behaviors during simulations. **a** Surface of an *in silico* tissue. Cell–cell boundaries (gray area) are observed in a cross-section. A reference surface (orange area) of the ith cell is defined on the tissue surface (blue area). **b** Dividing plane determined so as to be normal to tissue surfaces. The ith cell (white area) is divided by the ith dividing plane (brown area). The ith dividing plane passes through the center of inertia of the ith cell volume, denoted by $\boldsymbol{g}_i^{\text{c}}$. In addition, if the ith cell includes a reference surface (orange area), the ith dividing plane is determined so as to be along vector $\boldsymbol{d}_i^{\text{ref surf}}$. The vector $\boldsymbol{d}_i^{\text{ref surf}}$ is defined as the vector from $\boldsymbol{g}_i^{\text{c}}$ to the center point of the reference surface at the ith cell, denoted by $\boldsymbol{r}_i^{\text{ref surf}}$. **c** Equilibrium volume of the ith cell as a function of the ith cell time, denoted by $v_{\text{eq}\ i}^{\text{c}}(t_i^{\text{c}})$, as described by Eq. (10). A cell cycle period is separated into four states: I (blue), II (gray), III (light brown), and IV (dark brown). The ith cell divides when t_i^{c} is at the ith cell division time, denoted by $\tau_i^{\text{cell div}}$.

Global regulation: The directions of cell divisions are determined to be globally aligned within a whole tissue. Here, the x-axis is set to be the normal direction of dividing plane, and a unit vector along the x-axis is denoted by $\boldsymbol{u}_{\text{x}}$. To reflect the global directionality into cell division directions, vector $\boldsymbol{d}_i^{\text{cell div}}$ is given for cases $\Omega_i^{\text{ref surf}}$ and $\overline{\Omega}_i^{\text{ref surf}}$. For case $\Omega_i^{\text{ref surf}}$, vector $\boldsymbol{d}_i^{\text{cell div}}$ is a vector of $\boldsymbol{u}_{\text{x}}$ projected onto a plane normal to $\boldsymbol{d}_i^{\text{ref surf}}$. For case $\overline{\Omega}_i^{\text{ref surf}}$, vector $\boldsymbol{d}_i^{\text{cell div}}$ is $\boldsymbol{u}_{\text{x}}$.

3.2 Cell potential energy

To demonstrate simulations using our proposed model, cell potential energy was simply expressed using the potential energy by

$$U^{\text{total}} = U^{\text{cv}} + U^{\text{cs}} + U^{\text{cc}}, \tag{8}$$

where U^{cv} indicates cell volume elasticity, U^{cs} is cell surface elasticity, and U^{cc} is cell–cell adhesion. Here, U^{cv} and U^{cs} are categorized by U^{cell}, and U^{cc} is categorized by $U^{\text{cell–cell}}$ in Eq. (2).

3.2.1 Cell volume elasticity

To express cell volume elasticity, the current volume of the ith cell, $v_i^{\text{c}}(t_i^{\text{c}})$, was introduced. Then, cell volume elasticity, U^{cv}, was expressed by

$$U^{\text{cv}}(v_i^{\text{c}}) = \sum_i^{\text{cell}} \frac{1}{2} k^{\text{cv}} \left(\frac{v_i^{\text{c}}}{v_{\text{eq}\ i}^{\text{c}}} - 1 \right)^2, \tag{9}$$

which is similar to that employed in studies of other vertex models (Farhadifar et al. 2007; Honda et al. 2004, 2008a,b). Here $\sum_i^{\text{cell}}$ indicates the summation for all cells. The constant k^{cv} indicates volume elasticity. The variable $v_{\text{eq}\ i}^{\text{c}}$ indicates an equilibrium volume of the ith cell as a function of the ith cell time t_i^{c}.

The equilibrium cell volume of the ith cell $v_{\text{eq}\ i}^{\text{c}}$ increased continuously according to the ith cell time t_i^{c} (Fig. 2c):

$$\frac{v_{\text{eq}\ i}^{\text{c}}(t_i^{\text{c}})}{v_0^{\text{c}}} = \begin{cases} 0.75 + 0.25 \frac{t_i^{\text{c}}}{\psi^{\text{I}} \tau_i^{\text{cell div}}} & \text{in state I} \\ 1.0 & \text{in state II} \\ 1.0 + 0.5 \frac{t_i^{\text{c}} - (\psi^{\text{I}} + \psi^{\text{II}}) \tau_i^{\text{cell div}}}{\psi^{\text{III}} \tau_i^{\text{cell div}}} & \text{in state III} \\ 1.5 & \text{in state IV} \end{cases}. \tag{10}$$

Here, the constant v_0^{c} indicates a characteristic cell volume.

3.2.2 Cell surface elasticity

To express cell surface elasticity, a current surface of the ith cell, $s_i^{\text{c}}(t_i^{\text{c}})$, was introduced. Then, cell surface elasticity, U^{cs}, was expressed by

$$U^{\text{cs}}(s_i^{\text{c}}) = \sum_i^{\text{cell}} \frac{1}{2} k^{\text{cs}} \left(\frac{s_i^{\text{c}}}{s_{\text{eq}\ i}^{\text{c}}} - 1 \right)^2, \tag{11}$$

which is similar to that employed in studies of modeling cell membranes (Noguchi and Gompper 2005; Ujihara

et al. 2010). Here, the constant k^{cs} indicates surface elasticity. The variable $s^{\mathrm{c}}_{\mathrm{eq}\ i}$ indicates an equilibrium surface area of the ith cell. Assuming that an equilibrium state of cell shape is spherical, variable $s^{\mathrm{c}}_{\mathrm{eq}\ i}$ is defined by

$$s^{\mathrm{c}}_{\mathrm{eq}\ i} = 4\pi \left(\frac{3v^{\mathrm{c}}_{\mathrm{eq}\ i}}{4\pi} \right)^{\frac{2}{3}}. \tag{12}$$

Because Eq. (12) indicates a surface area of an equivalent sphere with the same volume, cell shapes tend to be spherical because of the force balance between the cell volume and surface elasticity in Eqs. (9) and (11).

3.2.3 Cell–cell adhesion

To express cell–cell adhesion, the boundary area between the ith and jth cells s^{cc}_{ij} was introduced. Then, cell–cell adhesion, U^{cc}, was expressed by

$$U^{\mathrm{cc}}\left(s^{\mathrm{cc}}_{ij}\right) = \sum_{i}^{\mathrm{cell}} \sum_{j(>i)}^{\mathrm{cell}} \epsilon^{\mathrm{cc}} s^{\mathrm{cc}}_{ij}, \tag{13}$$

which is similar to that employed in studies of other vertex models (Farhadifar et al. 2007; Honda et al. 2004, 2008a,b; Okuda et al. 2012). Here the constant ϵ^{cc} indicates the interface energy density between cells.

4 Simulating the morphodynamics of growing tissues

4.1 Simulation conditions

To establish that our proposed model can be applied to simulating tissue morphogenesis that involves cell proliferation, we simulated the morphodynamics of growing tissues. To resolve Eq. (1), parameter values were normalized by unit length (l), unit time (τ), and unit energy (k_BT). Here l and τ were set as $l = (v_0)^{\frac{1}{3}}$ and $\tau = \eta\,(v_0)^{\frac{2}{3}}/k_BT$.

As an initial condition, proliferating cells were located as in a monolayer sheet on a spherical shell (Fig. 3). The number of proliferating cells under this initial condition was set to $n^{\mathrm{c}}_0 = 18$. Reference surfaces of cell divisions (colored in orange in Fig. 3) are defined as polygonal faces between boundary cells and the extracellular space outside the spherical tissue. Each cell time, t^{c}_i, under the initial condition is randomly determined to satisfy $< t^{\mathrm{c}}_i >_0 = 0.1\tau^{\mathrm{cell\ cycle}}_{\mathrm{ave}}$. Here $< \ldots >_0$ indicates the statistical average at $t = 0$. To equilibrate tissue shapes, tissue dynamics were calculated within a normalized time period of 1000 without cell division and growth. To obtain the statistical behaviors, five random samples were calculated in these simulations.

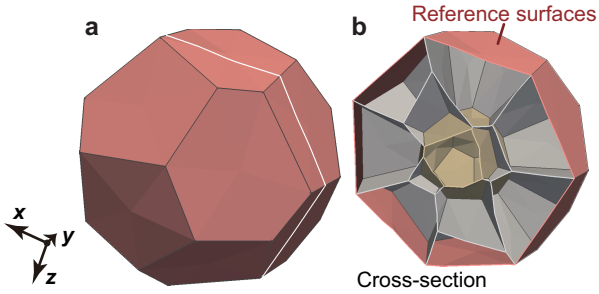

Fig. 3 Initial conditions for simulating tissue growth. **a** Shape of the entire growing tissue under the initial conditions. **b** Cross-section of the tissue cut at the white line shown in (**a**). Reference surfaces (orange areas) are defined as polygonal faces between cells and the extracellular space outside of the tissue. The tissue is a hollow shell with inner surfaces (yellow areas) and has a monolayer structure.

To establish that various timings and directionalities of cell division could be taken into account in our proposed model, cell division directions were determined under either the local or global regulation, as shown in Sect. 3.1, and average cell division times varied by $\tau^{\mathrm{cell\ cycle}}_{\mathrm{ave}} = 37.5$, 75.0, 150, 300, and 600. The standard deviation of cell division times $\tau^{\mathrm{cell\ cycle}}_{\mathrm{sd}}$ was set at $0.1\tau^{\mathrm{cell\ cycle}}_{\mathrm{ave}}$. Time integration of Eq. (1) was numerically performed using the improved Euler method with a time step of Δt. Local network patterns were reconnected when each edge included in a local pattern became shorter than a threshold value, Δl_{th}. Trials for applying the reconnection rule were conducted for each edge and each trigonal face at each time interval of Δt_r. All model parameters are shown in Table 1.

4.2 Results

To establish that our proposed model could reflect proliferative cell behaviors during tissue growth, two basic quantities, cell volume and sphericity, representing cell size and shape were observed. Figure 4a shows the average cell volumes during tissue growth. Cell volumes were maintained at approximately $0.9v_0$ during tissue growth under both the local and global regulations. Figure 4b shows the average cell sphericities during tissue growth. Cell sphericity is defined as the ratio of the radius of an equivalent sphere with the cell volume divided by that of the cell surface area. Cell sphericities were maintained at approximately 0.75 during tissue growth under both the local and global regulations. From these results, it was established that cell size and shape were maintained during tissue growth.

Table 1 Model parameters

Symbol	Value	Description
Physical parameters for cell mechanical properties		
η	1.0	Friction coefficient of vertex
k^{cv}	20	Constant of cell volume elasticity
k^{cs}	2.56	Constant of cell surface elasticity
ϵ^{cc}	-0.01	Interface energy at cell–cell boundaries
v_0	1.0	Characteristic cell volume
$\tau_{\mathrm{ave}}^{\mathrm{cell\ cycle}}$	$37.5 - 600$	Statistical average of cell cycle
ψ^{I}	0.6	Time ratio of state I
ψ^{II}	0.2	Time ratio of state II
ψ^{III}	0.1	Time ratio of state III
ψ^{IV}	0.1	Time ratio of state IV
Numerical parameters for computational simulations		
Δt	0.001	Integration time step
Δt_{r}	0.002	Time interval of network reconnections
Δl_{th}	0.05	Threshold length of network reconnections

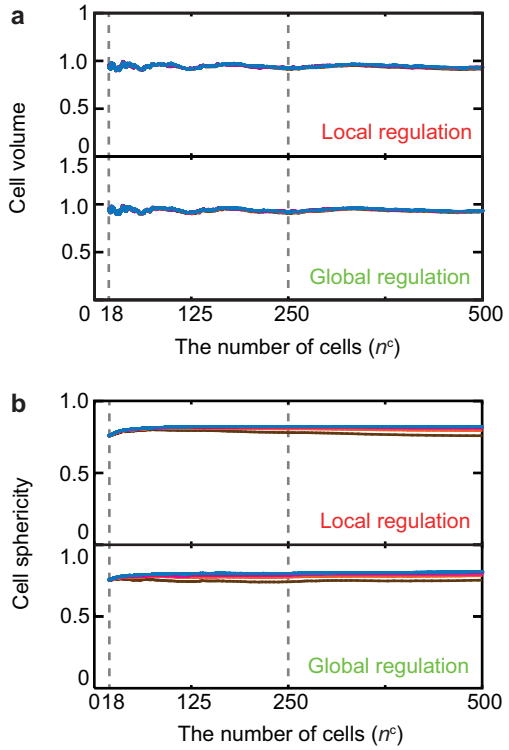

Fig. 4 Average cell size and shape. **a** Cell volume as a function of the number of cells under local (upper) and global (lower) regulations. **b** Cell sphericity as a function of the number of cells under local (upper) and global (lower) regulations. Line colors indicate the conditions: $\tau_{\mathrm{ave}}^{\mathrm{cell\ cycle}} = 37.5$ (brown), 75.0 (orange), 150 (pink), 300 (purple), and 600 (blue). Gray dashed lines indicate the states: $n^{\mathrm{c}} = 18$ and 250.

Figure 5 shows the morphogenesis of growing tissues induced by successive rounds of cell proliferation. The graphs in Fig. 5a and b show the cell number as a function of time under the local and global regulations, respectively. Black lines in these graphs indicate the theoretical solution

$$n^{\mathrm{c}}(t) = n_0^{\mathrm{c}} \cdot 2^{\frac{t+<t_i^{\mathrm{c}}>_0}{\tau_{\mathrm{ave}}^{\mathrm{cell\ cycle}}}}, \tag{14}$$

where n_0^{c} and $< t_i^{\mathrm{c}} >_0$ indicate the number of cells and the mean of cell times at $t = 0$, respectively. Under each condition of the cell cycle $\tau_{\mathrm{ave}}^{\mathrm{cell\ cycle}}$, the increases in the number of cells obeyed the theoretical solution shown in Eq. (14) within the given standard deviation $\tau_i^{\mathrm{cell\ div}}$ shown in Eq. (7).

Tissues grew with time as shown in the whole views in Fig. 5a and b (see also Movies 1 and 2 in the Supplemental data). Tissue shapes under the local regulation deformed without anisotropy and remained rather spherical (Fig. 5a). In contrast, tissue shapes under the global regulation deformed to become cylindrical (Fig. 5b). Although there were no conditions that constrained the layer structures of tissues, tissues under the local regulation maintained most of their monolayer structure, as shown in the cross-section view in Fig. 5a. In contrast, tissues under the global regulation adopted multilayer structures at several locations, as shown in the cross-section view in Fig. 5b. Friction forces generated by cell movements resulted in forming these multilayer structures. Because cells move along the direction of the tissue elongation, these friction forces work as compressive forces on the tissue. Under the compressive conditions, cells are pushed out of the plane of cell sheet so as to form multilayer structures.

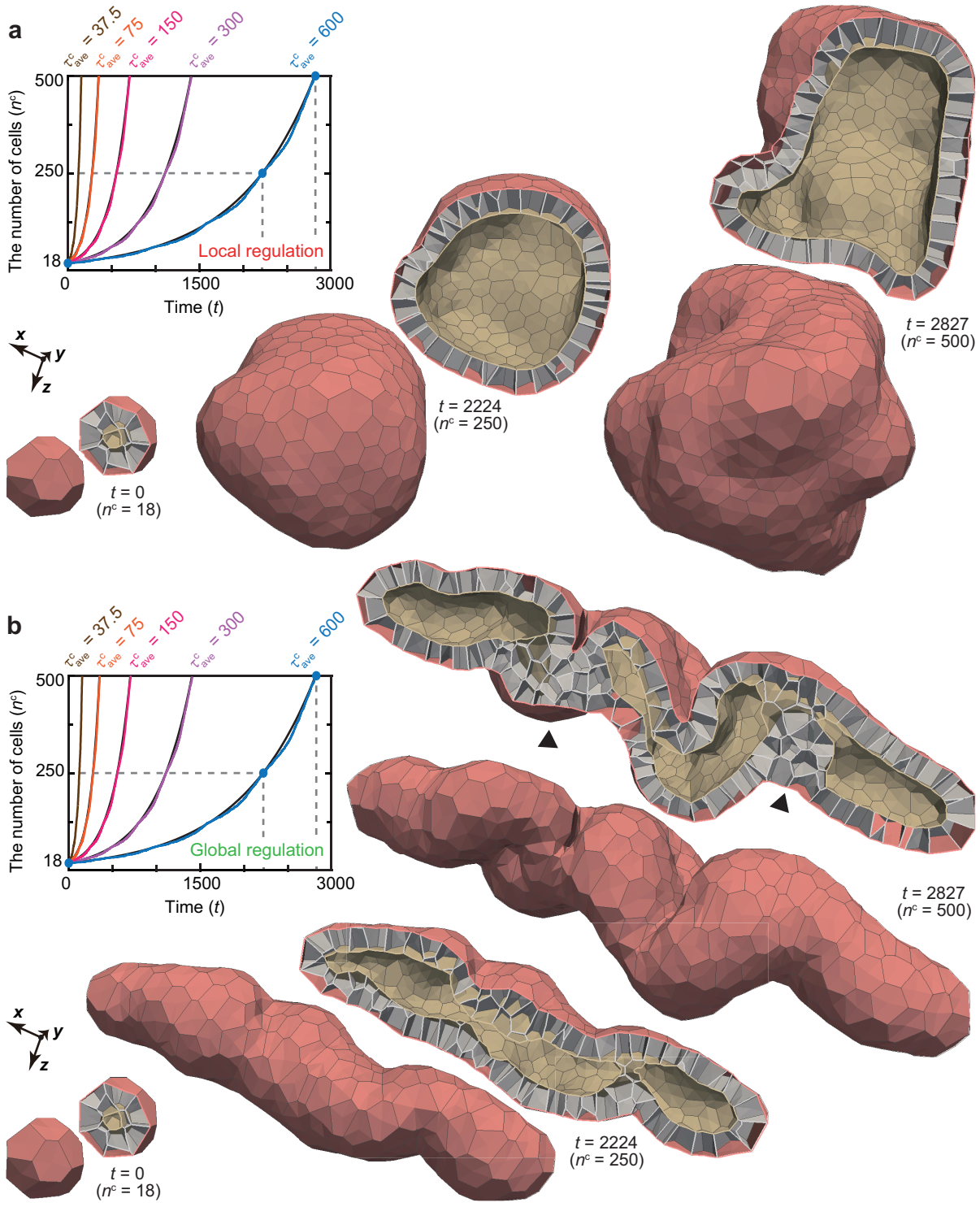

Fig. 5 Tissue growth as a result of cell proliferation. **(a)** Simulation results under the local regulation. **(b)** Simulation results under the global regulation. **Graphs**: Number of cells as a function of time under the local and global regulations. Line colors indicate the conditions: $\tau_{\rm ave}^{\rm cell\ cycle} = 37.5$ (brown), 75.0 (orange), 150 (pink), 300 (purple), and 600 (blue). Black lines indicate theoretical solutions of Eq. (14). **Illustrations**: Snapshots of whole and cross-section views of growing tissues at $t = 0$, 2224, and 2827 (in order from left). These tissues include cell numbers $n^{\rm c} = 18$, 250, and 500 (gray dashed lines in Graphs), respectively. While tissues under the local regulation maintained a monolayer structure in (**a**), those under the global regulation included some multilayer structures as indicated by black triangles in (**b**). These morphogenetic processes under the local and global regulations are also shown in Movies 1 and 2 in the Supplemental data, respectively.

5 Discussion

5.1 Expression of proliferative cell behaviors based on a RNR framework

In our simulations, tissues grew with time in which the numbers of cells increased (Fig. 5) and cell size and shape were maintained (Fig. 4). Furthermore, tissue morphology dramatically differed based on the regulation used for providing the cell division direction: spherical shape with a monolayer structure under the local regulation and a trabecular shape with partially multilayer structures under the global regulation. From these results, our proposed model successfully reflected the fundamental behaviors of proliferating cells based on a RNR model framework.

5.2 Anticipated applications of our proposed model

In our simulations, timing ($\tau_i^{\text{cell div}}$), intracellular position ($\boldsymbol{c}_i^{\text{cell div}}$), and direction of cell division ($\boldsymbol{d}_i^{\text{cell div}}$) described in Sect. 2.2 were provided under the following assumptions. (1) Timing of cell division was independent of a cell mechanical state. (2) Cell division was symmetric. (3) Direction of cell division was provided according to either a local or a global regulation. In general, these assumptions were not always necessary for our proposed model. We emphasize that $\tau_i^{\text{cell div}}$, $\boldsymbol{c}_i^{\text{cell div}}$, and $\boldsymbol{d}_i^{\text{cell div}}$ are entirely arbitrary. Therefore, regulating $\tau_i^{\text{cell div}}$, $\boldsymbol{c}_i^{\text{cell div}}$, and $\boldsymbol{d}_i^{\text{cell div}}$, our proposed model could be applied to various behaviors of cell division. For example, simultaneous cell divisions can be expressed by giving $\tau_i^{\text{cell div}}$ the same timing among multiple cells. Asymmetric cell divisions can be expressed by giving $\boldsymbol{c}_i^{\text{cell div}}$ a position vector that deviates from the center of inertia of a cell, denoted by $\boldsymbol{g}_i^{\text{c}}$.

Although the time variances of cell mechanical properties and reference states were simply expressed in these simulations (Sect. 3.2), these can be expressed in more detail based on a different time scale. For example, the process of cell division is not a sudden, but a gradual progression during mitosis: a single cell gradually separates into two daughter cells as a spindle and contractile ring are produced. During this process, cell mechanical properties and reference states also gradually vary with time. These details can be reflected by choosing proper potential energy functions $U(\{t_i^{\text{c}}\})$ in Eq. (8).

Mechanical feedback in proliferative cell behaviors could have an important role during tissue morphogenesis. For example, active stress generated by cell activities, such as apical constriction in epithelial sheet, is transferred to surrounding cells. This stress may provide the surrounding cells with a feedback signal and regulate cell division (Woolner and Papalopulu 2012; Shraiman 2005). In our proposed model, a mechanical feedback system could also be implemented by designing different $U(\{t_i^{\text{c}}\})$ in Eq. (8) and coupling $\tau_i^{\text{cell div}}$, $\boldsymbol{c}_i^{\text{cell div}}$, and $\boldsymbol{d}_i^{\text{cell div}}$ described in Sect. 2.2 with biochemical and mechanical quantities.

5.3 Applicable areas of our proposed model

In principle, detailed expressions of proliferative cell behaviors at the subcellular scale are limited in our proposed model. For example, during mitosis, cell mechanical properties become inhomogeneous at the subcellular scale because of oriented configurations of stress fibers and the division spindle. These inhomogeneities in mechanical properties at the subcellular scale cannot be expressed. This is because our proposed model can only express proliferative cell behaviors over a range of length scales no larger than a polygonal face, which is the minimum unit comprising cell shapes in the RNR model. Mechanical forces of the contractile ring that pinch cell shape during mitosis are possible candidates to be used in our proposed model. For example, these effects could be expressed by introducing a potential energy that decreases a contour length of a dividing polygonal face similar to actomyosin contraction at apical junctions, as expressed in 2D vertex model (Farhadifar et al. 2007). Thus, when employing the proposed model to explain how subcellular inhomogeneities affect tissue morphogenesis, one possibility is to borrow the potential energy such as that given in the 2D vertex model.

To perform quantitative analysis using our proposed model, the cell mechanical properties that we assumed in our simulations need to be validated. In our proposed model, morphologies of cells and tissues depend on cell mechanics expressed by U in Eq. (2). For example, if the cell surface elasticity was decreased or excluded, cells would be flaccid. Because cell proliferation induces pushing forces exerted on cells in the plane of tissue sheet, cells would elongate perpendicular to the plane. Hence, tissue thickness would be larger. In general, because cell shape is resulted from the force balance in total cell mechanics, cell shape can be expressed by adjusting cell mechanics, such as elongated cell shapes in Drosophila wings (Farhadifar et al. 2007). To perform quantitative analysis, it will be necessary to experimentally measure cell mechanical properties during tissue morphogenesis, and a function of U and parameter values should be carefully chosen based on their contributions.

5.4 Future perspectives

Our proposed model can be used to simulate multicellular dynamics involving cell proliferation in 3D space based on the mechanical forces through cell–cell boundaries. Our proposed model will be an aid in understanding the mechanics of tissue morphogenesis involving cell proliferation, and in particular, the relationships between multicellular dynamics and tissue morphogenesis. Using our proposed model, we attempted to analyze the mechanical functions of characteristic behaviors of proliferating cells during tissue morphogenesis. Understanding these functions of cell proliferation is necessary to provide a comprehensive understanding of tissue morphogenesis and will become fundamental knowledge for controlling tissue morphogenesis in tissue engineering. Furthermore, general validation of our proposed model warrants certain predictions for the morphogenetic processes of tissues and even organs. Thus, our proposed model will contribute to exploring the frontiers of developmental biomechanics.

6 Conclusions

To analyze the mechanical effects of the proliferative cell behaviors of cell division and growth on tissue morphogenesis, we model cell proliferation based on a RNR model framework. In our proposed model, cell division was expressed by dividing a polyhedron at a planar surface for which cell division behaviors were characterized by three quantities: timing, intracellular position, and direction of the dividing plane. In addition, cell growth was expressed by potential energy as a function of individual cell times within their respective cell cycles. To establish that proliferative cell behaviors can be expressed, the morphodynamics of growing tissues were simulated. Based on these results, tissues grew with time, wherein the numbers of cells increased and the average cell size and shape were maintained. Furthermore, tissue morphology was dramatically different based on the regulations for providing the cell division direction. From these results, our proposed model successfully expressed proliferative cell behaviors based on a RNR model framework. Using our proposed model, we attempted to determine the general effects of proliferative cell behaviors on tissue morphogenesis at a scale of multiple cells.

Acknowledgements This work was partially supported by the Funding Program for Next Generation World-Leading Researchers (LR017) from the Ministry of Education, Culture, Sports, Science and Technology (MEXT) in Japan. Satoru Okuda was supported by the Japan Society for the Promotion of Science (JSPS) as a JSPS fellow. Yasuhiro Inoue was supported by "Morphologic" Grant-in-Aid for Scientific Research on Innovative Areas (23127506) from the MEXT in Japan.

References

Baena-López LA, Baonza A et al (2005). "The orientation of cell divisions determines the shape of Drosophila organs." Curr Biol 15(18): 1640-1644

Davies JA (2005). "Mechanisms of morphogenesis: the creation of biological form." Elsevier Academic Press, Burlington, New York

Eiraku M, Adachi T et al (2012). "Relaxation-expansion model for self-driven retinal morphogenesis." Bioessays 34(1): 17-25

Eiraku M, Takata N et al (2011). "Self-organizing optic-cup morphogenesis in three-dimensional culture." Nature 472(7341): 51-56

Farhadifar R, Röper JC et al (2007). "The influence of cell mechanics, cell–cell interactions, and proliferation on epithelial packing." Curr Biol 17(24): 2095-2104

Friedlander DR, Mège RM et al (1989). "Cell sorting-out is modulated by both the specificity and amount of different cell-adhesion molecules (CAMs) expressed on cell-surfaces." Proc Natl Acad Sci U S A 86(18): 7043-7047

Gibson WT, Veldhuis JH et al (2011). "Control of the mitotic cleavage plane by local epithelial topology." Cell 144(3): 427-438

Gong Y, Fraser C Mo SE (2004). "Planar cell polarity signalling controls cell division orientation during zebrafish gastrulation." Nature 430: 689-693

Heisenberg CP, Tada M et al (2000). "Silberblick/Wnt11 mediates convergent extension movements during zebrafish gastrulation." Nature 405: 76-81

Honda H, Yamanaka H (1984). "A computer simulation of geometrical configurations during cell division." J Theor Biol 106(3): 423-435

Honda H, Motosugi N et al (2008). "Computer simulation of emerging asymmetry in the mouse blastocyst." Development 135(8): 1407-1414

Honda H, Nagai T et al (2008). "Two different mechanisms of planar cell intercalation leading to tissue elongation." Dev Dyn 237(7): 1826-1836

Honda H, Tanemura M et al (2004). "A three-dimensional vertex dynamics cell model of space-filling polyhedra simulating cell behavior in a cell aggregate." J Theor Biol 226(4): 439-453

Ingber DE, Mammoto T (2010). "Mechanical control of tissue and organ development." Development 137(9): 1407-1420

Lechler T, Fuchs E (2005). "Asymmetric cell divisions promote stratification and differentiation of mammalian skin." Nature 437(7056): 275-280

Lecuit T, Lenne PF (2007). "Cell surface mechanics and the control of cell shape, tissue patterns and morphogenesis." Nat Rev Mol Cell Biol 8(8): 633-644

Lecuit T, Rauzi M et al (2008). "Nature and anisotropy of cortical forces orienting Drosophila tissue morphogenesis." Nat Cell Biol 10(12): 1401-1410

Lecuit T, Rauzi M et al (2010). "Planar polarized actomyosin contractile flows control epithelial junction remodelling." Nature 468(7327): 1110-1114

Noguchi H, Gompper G (2005). "Dynamics of fluid vesicles in shear flow: Effect of membrane viscosity and thermal fluctuations." Phys Rev E 72(1):11901-11914

Okuda S, Inoue Y et al "Reversible network reconnection model for simulating large deformation in dynamic tissue morphogenesis." Biomech Model Mechanobiol (in press)

Rauzi M, Verant P et al (2008). "Nature and anisotropy of cortical forces orienting Drosophila tissue morphogenesis." Nat Cell Biol 10(12): 1401-1410

Reddy GV, Heisler MG et al (2004). "Real-time lineage analysis reveals oriented cell divisions associated with morphogenesis at the shoot apex of Arabidopsis thaliana." Development 131: 4225-4237

Staple DB, Farhadifar R et al (2010). "Mechanics and remodelling of cell packings in epithelia." Eur Phys J E Soft Matter 33(2): 117-127

Ujihara Y, Nakamura M et al (2005). "Proposed Spring Network Cell Model Based on a Minimum Energy Concept." Ann Biomed Eng 38(4):1530-1538

Poulson ND, Lechler T (2010). "Robust control of mitotic spindle orientation in the developing epidermis." J Cell Biol 191(5): 915-922

Shraiman BI (2005). "Mechanical feedback as a possible regulator of tissue growth." Proc Natl Acad Sci U S A 102(9): 3318-3323

Siller KH, Cabernard C et al (2006). "The NuMA-related Mud protein binds Pins and regulates spindle orientation in Drosophila neuroblasts." Nat Cell Biol 8(6): 594-600

Taniguchi K, Maeda R et al (2011). "Chirality in planar cell shape contributes to left-right asymmetric epithelial morphogenesis." Science 333(6040): 339-341

Weliky M, Oster G (1990). "The mechanical basis of cell rearrangement. 1. Epithelial morphogenesis during fundulus epiboly." Development 109(2): 373-386

Woolner S, Papalopulu N (2012). "Spindle Position in Symmetric Cell Divisions during Epiboly Is Controlled by Opposing and Dynamic Apicobasal Forces." Dev Cell 22(4): 775-787